IEEE Access
Multidisciplinary | Rapid Review | Open Access Journal

Received 2 August 2022, accepted 18 August 2022, date of publication 23 August 2022, date of current version 29 August 2022.

Digital Object Identifier 10.1109/ACCESS.2022.3201134

RESEARCH ARTICLE

A Novel Modulation-Based Current Harmonic Control Strategy for PMSM Considering Current Measurement Error and Asymmetric Impedance

HAO LIN[1], YONG LIAO[1,2], LUOCHENG YAN[3], FU LI[4], AND YIXIAO FENG[1]

[1]School of Electrical Engineering, Chongqing University, Chongqing 400044, China
[2]State Key Laboratory of Power Transmission Equipment and System Security and New Technology, Chongqing University, Chongqing 400044, China
[3]Department of Electronic and Electrical Engineering, The University of Sheffield, Sheffield S1 3JD, U.K.
[4]College of Automation and Electronic Information, Xiangtan University, Hunan 411105, China

Corresponding author: Hao Lin (haolin@cqu.edu.cn)

ABSTRACT The permanent magnet synchronous machines system includes various harmonics caused by asymmetric impedance, current measurement errors, spatial harmonics, and inverter nonlinearity. The asymmetric impedance and the current measurement scaling error cause an asymmetry among three-phase currents, which produces a negative-sequence fundamental current. The controller cannot distinguish between their effects and reduce asymmetric currents. Therefore, a novel modulation-based current harmonic control strategy is proposed in this paper. The complex-vector system model accounting for these harmonics is established to illustrate the modulation effects of motor saliency, the asymmetric impedance, and the current measurement scaling error. According to modulation principles, the actual negative-sequence fundamental current is reconstructed to suppress the harmonic current caused by the asymmetric impedance. Meanwhile, the measured negative-sequence fundamental current is employed to compensate for the scaling error, and the DC component of current measurements is employed to compensate for the offset. The harmonic current controller also suppresses other harmonic currents. The harmonic current controller and the current measurement compensator based on the complex vector control are designed. Experiments verify the correctness and feasibility of the proposed control strategy.

INDEX TERMS Permanent magnet synchronous machine (PMSM), current harmonic, asymmetric impedance, current measurement error.

I. INTRODUCTION

Permanent magnet synchronous machines (PMSMs) are applied to various industrial applications due to the advantages of high torque density, high power density, and high efficiency [1], [2]. In control systems of PMSMs, both the spatial harmonics from the machine side and the nonlinearity from the inverter side contribute to voltage disturbances of harmonic frequencies [3], [4]. In addition, the asymmetric impedance among three phases and the current measurement errors, i.e., offset and scaling errors, introduce impedance disturbances [5] and measurement disturbances [6], respectively. Since all these disturbances can generate related current harmonics and torque ripples, different control approaches are employed to suppress or inject the current harmonics caused by different disturbance sources. The harmonic control further achieves better control performance, such as reduced harmonic losses, reduced torque ripples, and boosted average torque [4], [7].

In terms of the voltage harmonics due to the machine and inverter, there are various proposals about how to compensate for the effect of those harmonics. The basic control

The associate editor coordinating the review of this manuscript and approving it for publication was Shaopeng Wu.

principle is to inject related voltage harmonics and counterbalance the voltage harmonics. Reference [8] proposes multiple proportional-integral (PI) regulators in multiple synchronous frames (MSFs) to regulate current harmonics and track the optimized current harmonic references to reduce the torque ripples. To avoid the interference among different frequencies, current harmonics should usually be extracted by using digital low-pass filter (LPF) techniques in MSFs. To improve the performance of current harmonic extraction, compared to the conventional digital LPFs, many papers proposed more advanced filtering methods under the framework of MSFs. A high-precision close-loop detection system is proposed in [9] to extract the selective current harmonic with a reduced delay effect, but the order of the system increases as well. Reference [10] employs an adaptive filter based on the least mean square to extract the current harmonics. Because the adaptive filter provides adaptive attenuation on the current components in other frequencies, the filter bandwidth does not need to change with the motor speed, unlike the conventional LPFs. Reference [11] reports a virtual multiphase system to extract the current harmonics. The phase shifting operation is employed to establish the virtual multiphase currents, based on which the vector space decomposition technique is then utilized to separate all the current harmonics. Since no digital filter is used in the current harmonic extraction, the delay effect is significantly reduced, which improves dynamic performance and system stability. Although these MSF-based methods above provide reasonable solutions to the suppression and injection of current harmonics in PMSM systems, the controller design and parameter tuning persist in the conventional ways of PI regulators, which limits the control performance on current harmonics and restricts the applicability of the MSF-based methods.

Reference [12] extended the PI regulators in MSF to the proportional-resonant (PR) regulator in a stationary frame, and [13] compensated the gain of the discrete regulator near the resonant frequency by using zero pole correction, which makes the PR regulator widely utilized in the current harmonic regulation of electrical machine [14], [15]. Compared to the PI regulator in MSFs, the PR regulator shows less computation burden but more complicated parameter tuning due to the interferences among different frequencies [14]. Except for the two basic regulators above, other methods also exhibit good performance on current harmonic control, such as the repetitive controller proposed in [16], the adaptive filter for dead-time compensation in [17], and the adaptive linear neuron studied in [18].

In terms of the current measurement disturbance, off-line correction can reduce the effect of the current measurement errors. However, due to temperature and operating condition variations, the current measurement errors are still required to be compensated online. Reference [19] proposed a novel current measurement topology, based on which multiple current sampling in one PWM cycle can be used to correct the offset and scaling errors. However, this method requires hardware modification, which will increase the cost of a control system. Since the current measurement errors will generate current harmonics in the control system, the errors can be compensated by extracting the related current harmonics [20], [21]. Reference [22] extracts the related voltage harmonics from the output voltage to compensate for the current measurement errors. Reference [23] injects high-frequency voltage and extracts the related current harmonics to compensate for current measurement errors.

In terms of the impedance due to asymmetry among the three phases, the basic control principle is also to inject related voltage harmonics and counterbalance the impedance disturbances. The asymmetric impedance causes an asymmetry among the existing current to produce more voltage and current harmonics. MSF-based method [24] and PR regulator [25] are also employed to suppress the harmonic current generated by the asymmetric impedance. Furthermore, the asymmetric resistances are estimated by recursive least squares to compensate for the asymmetric voltages in [5].

There are different harmonics in the motor system. The harmonic control can suppress the harmonic currents caused by different sources. Due to the asymmetric impedance, the fundamental current becomes asymmetrical, which produces a negative-sequence fundamental current. Control of this harmonic current can reduce the asymmetrical voltage. The offset and scaling errors of the current measurement also introduce corresponding harmonic currents through the controller. These harmonic currents are also employed to compensate for the current measurement errors. However, the asymmetric impedance and the scaling error both result in an asymmetry of the fundamental current, which produces the same negative-sequence fundamental current. The controller cannot distinguish between the two sources. This harmonic cannot be employed to handle the asymmetric impedance and compensate for the scaling error at the same time. Therefore, a novel modulation-based current harmonic control strategy is proposed in this paper. When the saliency of motor exists (magnetic saturation can also have the saliency effect), the negative-sequence fundamental current will be modulated into a positive-sequence third harmonic current. The asymmetric impedance can be handled by using the positive-sequence third harmonic current. Meanwhile, the measured negative-sequence fundamental current is employed to compensate for the scaling error. The offset is compensated by the measured DC component. In addition, other harmonic currents are suppressed by the harmonic current controller. When the steady state is reached, the asymmetric impedance is handled, the current measurement errors are compensated, and the harmonic currents are suppressed.

The structure of this paper is organized as follows. In Section II, the system model considering spatial harmonics, the inverter nonlinearity, impedance asymmetry, and current measurement errors is established based on the complex vector method. Section III analyses the modulation principles of the asymmetry, motor saliency, and scaling error. The harmonic current controller and the measurement error compensator are designed based on the complex vector control.

Experiments in Section IV verify the effectiveness of the controller. Finally, Section V concludes the paper.

II. MOTOR SYSTEM MODEL

The vector and complex vector methods are equivalent in the motor system model [26]. In order to analyze the relationship between positive and negative sequence harmonics caused by the modulation, the mathematical model in this paper is developed by the complex vector method. The complex-vector 3-to-2 transformation is

$$\boldsymbol{F} = \frac{2}{3}\left(e^{-j\theta}F_A + e^{-\boldsymbol{j}\left(\theta-\frac{2}{3}\pi\right)}F_B + e^{-j\left(\theta+\frac{2}{3}\pi\right)}F_C\right) \quad (1)$$

where θ is an angular, F is the voltage, current, or flux linkage, and the subscripts "A," "B," and "C" indicate the phase axis. The bold $\boldsymbol{F}$ indicates the complex vector.

According to the complex vector transformation, we establish the motor system model, which includes various harmonics caused by the motor, inverter, and current measurement. Flux harmonics and asymmetric impedance can generate harmonics in the motor. The inverter also introduces voltage harmonics. The current measurement errors include offset and scaling errors, which can also produce harmonics. The motor system diagram is shown in Fig. 1, and the models are described in the following parts.

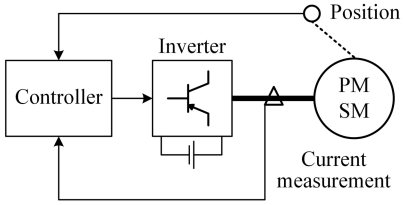

FIGURE 1. The motor system diagram.

A. MOTOR MODEL

The traditional complex vector motor model in a synchronous reference frame can be derived as

$$\begin{aligned} \boldsymbol{u}_{dq} &= r\boldsymbol{i}_{dq} + p\boldsymbol{\psi}_{dq} + j\omega_e\boldsymbol{\psi}_{dq} \\ \boldsymbol{\psi}_{dq} &= L_p\boldsymbol{i}_{dq} + L_s\boldsymbol{i}^*_{dq} + \boldsymbol{\psi}_f \\ T_e &= \frac{3}{4}jP\left(\boldsymbol{\psi}_{dq}\boldsymbol{i}^*_{dq} - \boldsymbol{\psi}^*_{dq}\boldsymbol{i}_{dq}\right) \end{aligned} \quad (2)$$

where $\boldsymbol{u}_{dq}$, $\boldsymbol{i}_{dq}$, ψ_{dq}, and ψ_f are complex vectors of voltage, current, flux linkage, and permanent magnet (PM) flux linkage in the synchronous frame, respectively; r is the stator resistance; T_e is the electromagnetic torque; P is pole pairs; ω_e is the electric angular velocity; p denotes a differential operator; the superscript $*$ indicates the conjugate of the complex vector; L_d is the d-axis inductance, and L_q is the q-axis inductance. Then the positive-sequence inductance L_p and the saliency inductance L_s can be expressed as

$$\begin{aligned} L_p &= = \frac{1}{2}\left(L_d + L_q\right) \\ L_s &= \frac{1}{2}\left(L_d - L_q\right) \end{aligned} \quad (3)$$

B. FLUX HARMONICS

Flux harmonics are mainly caused by motor spatial harmonics. Due to the influence of design, manufacture, and magnetic saturation, the air-gap flux density generated by the permanent magnets has the characteristics of the non-sinusoidal distribution. Thus the three-phase PM flux linkage can be expressed as

$$\begin{bmatrix} \psi_{fA} \\ \psi_{fB} \\ \psi_{fC} \end{bmatrix} = \sum \psi_{f(2n-1)} \begin{bmatrix} \cos\left(2N-1\right)\theta_e \\ \cos\left(2N-1\right)\left(\theta_e - \frac{2\pi}{3}\right) \\ \cos\left(2N-1\right)\left(\theta_e + \frac{2\pi}{3}\right) \end{bmatrix} \quad (4)$$

where N is a positive integer; $\psi_{f(2N\text{-}1)}$ is the magnitude of fundamental and harmonic components; θ_e is the electric angular.

Due to the symmetry of the air gap magnetic density distribution, the three-phase PM flux linkage includes odd-order harmonics flux linkage. According to the complex vector transformation, the PM flux linkage of the synchronous frame can be obtained as

$$\boldsymbol{\psi}_f = \psi_{f1} + \sum \psi_{f(6N-1)}e^{-j6N\theta_e} + \sum \psi_{f(6N+1)}e^{j6N\theta_e} \quad (5)$$

The PM flux linkage with orders of $3N$ in the three-phase system is the zero-sequence flux linkage. Through the transformation, there are only the fundamental PM flux linkage and the positive and negative sequence harmonic PM flux linkage with orders of $6N$ in the synchronous frame.

C. ASYMMETRIC IMPEDANCE

Motor manufacturing inevitably leads to an asymmetry among the three phases. As studied in [5], even a small asymmetric resistance can produce specific torque pulsation. Considering the asymmetry of resistance and taking phase C as the reference, the three-phase resistance is

$$\boldsymbol{R_{ABC}} = \begin{bmatrix} r & 0 & 0 \\ 0 & r & 0 \\ 0 & 0 & r \end{bmatrix} + \begin{bmatrix} r_1 & 0 & 0 \\ 0 & r_2 & 0 \\ 0 & 0 & 0 \end{bmatrix} \quad (6)$$

where r_1 and r_2 are asymmetric resistances of phases A and B.

Similarly, considering the inductance asymmetry and taking phase C as the reference, the three-phase inductance is

$$\begin{aligned} \boldsymbol{L_{ABC}} = &\begin{bmatrix} L_A & M_{AB} & M_{AC} \\ M_{AB} & L_B & M_{BC} \\ M_{AC} & M_{BC} & L_C \end{bmatrix} \\ &+ \begin{bmatrix} L_1 & M_{12} & M_{13} \\ M_{12} & L_2 & M_{23} \\ M_{13} & M_{23} & 0 \end{bmatrix} \end{aligned} \quad (7)$$

where L and M are self and mutual inductances; the subscript {ABC} indicates the three-phase normal condition, and the subscript {123} indicates the asymmetric condition.

Then the voltage and flux equations of the synchronous reference frame are deduced as

$$\begin{aligned} p\boldsymbol{\psi}_{dq} &= \boldsymbol{u}_{dq} - \boldsymbol{r}_p \boldsymbol{i}_{dq} - e^{-j2\theta_e}\boldsymbol{r}_n \boldsymbol{i}^*_{dq} \\ \boldsymbol{\psi}_{dq} &= \boldsymbol{l}_p \boldsymbol{i}_{dq} + L_s \boldsymbol{i}^*_{dq} + e^{-j2\theta_e}\boldsymbol{l}_n \boldsymbol{i}^*_{dq} + \boldsymbol{\psi}_f \end{aligned} \tag{8}$$

where $\boldsymbol{r}_p$ and $\boldsymbol{r}_{\mathrm{n}}$ are the asymmetric positive-sequence resistance and the asymmetric negative-sequence resistance, respectively; $\boldsymbol{l}_p$ and $\boldsymbol{l}_n$ are the asymmetric positive-sequence inductance and the asymmetric negative-sequence inductance, respectively. These parameters can be expressed as

$$\begin{aligned} \boldsymbol{r}_p &= r + \frac{1}{3}(r_1 + r_2) \\ \boldsymbol{r}_n &= \frac{1}{3}\left(r_1 + r_2 e^{-j\frac{2}{3}\pi}\right) \end{aligned} \tag{9}$$

$$\begin{aligned} \boldsymbol{l}_p &= L_p + \frac{1}{3}(L_1 + L_2 - M_{12} - M_{13} - M_{23}) \\ \boldsymbol{l}_n &= \frac{1}{3}\Big(L_1 + L_2 e^{-j\frac{2}{3}\pi} + 2M_{12}e^{j\frac{2}{3}\pi} \\ &\quad + 2M_{13}e^{-j\frac{2}{3}\pi} + 2M_{23}\Big) \end{aligned} \tag{10}$$

In the model of asymmetric impedance, the negative-sequence resistance and inductance can produce the negative-sequence fundamental current in the stationary frame through the conjugate of the complex vector fundamental current.

D. VOLTAGE HARMONICS OF INVERTER

The inverter nonlinearity introduces voltage harmonics. These harmonics are caused by the dead-time effect and voltage drops in power devices, which are equivalent to the square wave voltage related to the fundamental current. This voltage of phase A can be expressed as

$$u_{Ai} = \mathrm{V}_i sgn(i_A) = \frac{4\mathrm{V}_i}{\pi}\sum \frac{1}{2N-1}\sin(2N-1)\theta_e \tag{11}$$

where V_i is the voltage amplitude and sgn is the sign function.

The nonlinear voltage is composed of the harmonic voltages with odd orders of $2N$-1. The harmonic voltage of the synchronous frame can be obtained as

$$\boldsymbol{u}_i = \frac{4j\mathrm{V}_i}{\pi}\left(-1 + \sum \frac{1}{6N-1}e^{-j6N\theta_e} - \sum \frac{1}{6N+1}e^{j6N\theta_e}\right) \tag{12}$$

Similar to the PM flux linkage, there are the fundamental voltage and the positive and negative sequence harmonic voltages with orders of $6N$ in the synchronous frame.

E. CURRENT MEASUREMENT ERRORS

The current measurement errors include offset errors and scaling errors. Generally, the three-phase current is detected by two current sensors (Currents of phase A and B are measured). Then the measured three-phase current is

$$\begin{aligned} i_{Am} &= (1 + k_{A\Delta})\, i_A + i_{Adc} \\ i_{Bm} &= (1 + k_{B\Delta})\, i_B + i_{Bdc} \\ i_{Cm} &= -i_{Am} - i_{Bm} \end{aligned} \tag{13}$$

where $k_{A\Delta}$ and $k_{B\Delta}$ are scaling errors of phase A and B, respectively; i_{Adc} and i_{Bdc} are current offset errors of phase A and B, respectively; $k_\Delta = k_{A\Delta}$-$k_{B\Delta}$ is the difference of scaling errors.

According to the complex vector transformation, the measured current in the synchronous frame is derived as

$$\boldsymbol{i}_{dqm} = \boldsymbol{k}_p \boldsymbol{i}_{dq} + e^{-j2\theta_e}\boldsymbol{k}_n \boldsymbol{i}^*_{dq} + e^{-j\theta_e}\boldsymbol{i}_{\alpha\beta dc} \tag{14}$$

where $i_{\alpha\beta dc}$, $\boldsymbol{k}_p$, and $\boldsymbol{k}_n$ are the current offset error of the stationary $\alpha\beta$-reference frame, the positive-sequence scaling gain, and the negative-sequence scaling gain, respectively. These parameters can be expressed as

$$\begin{aligned} \boldsymbol{i}_{\alpha\beta dc} &= \frac{2}{3}\left((1-e^{-j\frac{2}{3}\pi})i_{Adc} + (e^{j\frac{2}{3}\pi} - e^{-j\frac{2}{3}\pi})i_{Bdc}\right) \\ \boldsymbol{k}_p &= 1 + \frac{1}{6}\left(k_{A\Delta} + k_{B\Delta} + (e^{j\frac{2}{3}\pi} - e^{-j\frac{2}{3}\pi})k_\Delta\right) \\ \boldsymbol{k}_n &= \frac{1}{3}\left((1-e^{-j\frac{2}{3}\pi})k_\Delta\right) \end{aligned} \tag{15}$$

In the stationary frame, the current offset error can produce the direct current, and the negative-sequence scaling gain can produce the negative-sequence fundamental current in the current measurement. Then corresponding harmonic currents in the motor are generated by the controller. Generally, the offset error and the negative-sequence scaling gain can be compensated by the corresponding harmonic current [22], [23]. The scaling error of the current measurement in the real system is not too large. Thus the error of the positive-sequence scaling gain is often treated as a parameter variation of the control system.

F. SYSTEM MODEL

When we consider flux harmonics, asymmetric impedance, harmonic voltages, and current measurement errors, the complex vector system model in the synchronous reference frame can be derived as

$$\begin{aligned} p\boldsymbol{\psi}_{dq} &= \boldsymbol{u}_{dq} + \boldsymbol{u}_i - \boldsymbol{r}_p \boldsymbol{i}_{dq} - e^{-j2\theta_e}\boldsymbol{r}_n \boldsymbol{i}^*_{dq} - j\omega_e \boldsymbol{\psi}_{dq} \\ \boldsymbol{\psi}_{dq} &= \boldsymbol{l}_p \boldsymbol{i}_{dq} + L_s \boldsymbol{i}^*_{dq} + e^{-j2\theta_e}\boldsymbol{l}_n \boldsymbol{i}^*_{dq} + \boldsymbol{\psi}_f \\ \boldsymbol{i}_{dqm} &= \boldsymbol{k}_p \boldsymbol{i}_{dq} + e^{-j2\theta_e}\boldsymbol{k}_n \boldsymbol{i}^*_{dq} + e^{-j\theta_e}\boldsymbol{i}_{\alpha\beta dc} \end{aligned} \tag{16}$$

In summary, flux harmonics, the asymmetric impedance, voltage harmonics of the inverter, and current measurement errors can lead to many harmonics in the motor. Parameters related to the electrical angular and the conjugate of the complex vector both represent the modulation effect. Therefore, we will analyze the modulation of harmonics in the next section.

III. PROPOSED CONTROL STRATEGY

This paper proposes a novel modulation-based current harmonic control strategy. The modulation of harmonics is analyzed by the harmonic balance method. Because the impedance asymmetry and the current measurement scaling error have the same modulation effect, it is difficult to identify the source of current harmonics. Usually, we cannot deal with

them at the same time. However, based on the modulation of motor saliency, the actual negative-sequence fundamental current can be reconstructed by the positive-sequence third harmonic current to reduce the effect of the impedance asymmetry. Meanwhile, flux harmonics and voltage harmonics of the inverter are suppressed by the harmonic current controller. In addition, the direct current and the measured negative sequence fundamental current are employed to compensate for the current measurement errors.

A. MODULATION OF HARMONICS

The principle of modulation effects is still unclear in the system model due to parameters related to the electrical angle. In the arbitrary frame, we can simplify the form of the model. The complex-vector transformation of the arbitrary frame is

$$\boldsymbol{F}_H = e^{j(1-H)\theta_e}\boldsymbol{F}_{dq} \tag{17}$$

where the subscript H denotes the arbitrary frame with the stationary frame as a reference.

Then the complex vector model of the arbitrary frame can be derived as

$$\begin{aligned} p\boldsymbol{\psi}_H &= \boldsymbol{u}_H + \boldsymbol{u}_{Hi} - \boldsymbol{r}_p\boldsymbol{i}_H - \boldsymbol{r}_n\boldsymbol{i}^*_{-H} - jH\omega_e\boldsymbol{\psi}_h \\ \boldsymbol{\psi}_H &= \boldsymbol{l}_p\boldsymbol{i}_H + L_s\boldsymbol{i}^*_{2-H} + \boldsymbol{l}_n\boldsymbol{i}^*_{-H} + e^{j(1-H)\theta_e}\boldsymbol{\psi}_f \\ \boldsymbol{i}_{Hm} &= \boldsymbol{k}_p\boldsymbol{i}_H + \boldsymbol{k}_n\boldsymbol{i}^*_{-H} + \boldsymbol{i}_{Hdc} \end{aligned} \tag{18}$$

where the relationship of parameters can be expressed as

$$\begin{aligned} \boldsymbol{i}_{Hdc} &= e^{-jH\theta_e}\boldsymbol{i}_{\alpha\beta dc} \\ \boldsymbol{u}_{Hi} &= e^{j(1-H)\theta_e}\boldsymbol{u}_i \end{aligned} \tag{19}$$

This model explains the modulation effects of motor saliency, impedance asymmetry, and current measurement scaling errors, especially the interaction mechanism of each harmonic. The impedance asymmetry and the scaling error have the same modulation effect. Due to the negative-sequence scaling gain, inductance, and resistance, the harmonic component in the $(-H)^{\text{th}}$ frame can influence the harmonic component in the H^{th} frame. Considering the modulation effects of the saliency, the harmonic component in the $(2-H)^{\text{th}}$ frame can influence the harmonic component in the H^{th} frame due to the saliency inductance. According to the model of the arbitrary frame, the relationship between harmonic components is analyzed by the harmonic balance method. Then, it is assumed that the positive and negative sequence current and voltage in the stationary frame are

$$\begin{aligned} \boldsymbol{I}_{\alpha\beta} &= \sum \boldsymbol{I}_h e^{jh\theta_e} \\ \boldsymbol{U}_{\alpha\beta} &= \sum \boldsymbol{U}_h e^{jh\theta_e} \end{aligned} \tag{20}$$

where the subscript h represents the harmonic order (the stationary frame is used as a reference), and the sign of h indicates the positive (>0) or negative (<0) sequence.

Substituting equation (20) into equation (18), the h^{th}-order harmonic model is obtained as

$$\boldsymbol{U}_h + \boldsymbol{U}_{hd} = \boldsymbol{Z}_{hp}\boldsymbol{I}_h + \boldsymbol{Z}_{hn}\boldsymbol{I}^*_{-h} + \boldsymbol{Z}_{hs}\boldsymbol{I}^*_{2-h} \tag{21}$$

where the subscripts p, n, and s represent the positive sequence, negative sequence, and saliency, respectively. $\boldsymbol{U}_{hd}$ is the h^{th}-order voltage harmonic, and the h^{th}-order harmonic impedance can be expressed as

$$\begin{aligned} \boldsymbol{Z}_{hp} &= \boldsymbol{r}_p + p\boldsymbol{l}_p + jh\omega_e\boldsymbol{l}_p \\ \boldsymbol{Z}_{hn} &= \boldsymbol{r}_n + p\boldsymbol{l}_n + jh\omega_e\boldsymbol{l}_n \\ \boldsymbol{Z}_{hs} &= pL_s + jh\omega_e L_s \end{aligned} \tag{22}$$

Voltage harmonics are caused by motor spatial harmonics and the inverter nonlinearity. The characteristic harmonic voltages can be obtained as (other harmonic voltages are zero and N is a positive integer)

$$\begin{aligned} \boldsymbol{U}_{1d} &= -\frac{4j\mathrm{V}_\Delta}{\pi} + j\omega_e\psi_{\psi f1} \\ \boldsymbol{U}_{(1-6\mathrm{N})d} &= \frac{4j\mathrm{V}_i}{\pi}\frac{1}{6N-1} - j(6N-1)\,\omega_e\psi_{f(6N-1)} \\ \boldsymbol{U}_{(6N+1)d} &= -\frac{4j\mathrm{V}_i}{\pi}\frac{1}{6N+1} + j(6N+1)\,\omega_e\psi_{f(6N+1)} \end{aligned} \tag{23}$$

Similarly, the measured harmonic current caused by current measurement errors can be obtained as

$$\boldsymbol{I}_{hm} = \boldsymbol{k}_p\boldsymbol{I}_h + \boldsymbol{k}_n\boldsymbol{I}^*_{-h} + \boldsymbol{I}_{hdc} \tag{24}$$

where $\boldsymbol{I}_{hdc}$ exists only when $h = 0$, which can be expressed as

$$\boldsymbol{I}_{0dc} = \boldsymbol{i}_{\alpha\beta dc} \tag{25}$$

In the harmonic model, the harmonic current is determined by the harmonic voltage source from the controller and the motor system. This harmonic voltage source introduces normal and modulated voltage harmonics of different harmonic impedances. Normal voltage harmonics are caused by spatial harmonics and the inverter nonlinearity, and modulated voltage harmonics are caused by the impedance asymmetry and the saliency. Due to the saliency impedance, the $(2-h)^{\text{th}}$-order harmonic current is modulated to produce the h^{th}-order harmonic voltage, which can influence the h^{th}-order harmonic current. Similarly, due to the negative sequence impedance, the $(-h)^{\text{th}}$-order harmonic current is modulated to produce the h^{th}-order harmonic voltage, which can influence the h^{th}-order harmonic current. In the current measurement, the $(-h)^{\text{th}}$-order harmonic current is also modulated due to the negative-sequence scaling gain, which can influence the h^{th}-order measured harmonic current. Meanwhile, the current measurement offset errors can introduce the direct current through the controller, resulting in many even-order harmonic currents modulated by harmonic impedances. Therefore, there are many harmonic currents in the controller and the motor system. The main orders of these harmonic current sources are 0, 1, -1, $(1-6N)$, and $(6N+1)$ in the stationary frame. Due to modulation effects, the direct current (DC) source (the order of harmonic is 0) produces the even-order harmonic currents, and other harmonic current sources produce the odd-order harmonic currents. The negative sequence and saliency impedances are small, and these

harmonic currents are smaller than the fundamental current. Thus, the amplitude of harmonic currents is reduced with the increase of the harmonic order after the modulation. The diagram of the harmonic distribution in the stationary frame is shown in Fig. 2.

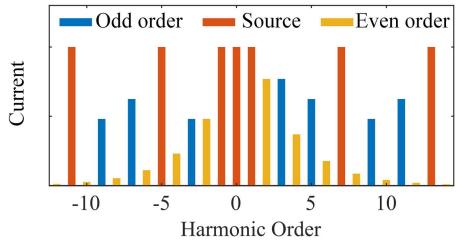

FIGURE 2. The diagram of the harmonic distribution in the stationary frame.

B. HARMONIC CURRENT RECONSTRUCTION

The fundamental current in the motor is the main component, modulated into various harmonics. It is challenging to use only the negative-sequence fundamental current to handle both the impedance asymmetry and the current measurement scaling error. Due to the modulation effect of motor saliency, the actual negative-sequence fundamental current is modulated into a positive-sequence third harmonic current. Then the actual negative-sequence fundamental current can be reconstructed by the positive-sequence third harmonic current. Therefore, this paper can handle the impedance asymmetry and the measurement scaling error separately. The impedance relationship of the related harmonics based on the harmonic model is obtained as

$$\begin{aligned} \boldsymbol{U}_{-1} &= \boldsymbol{Z}_{-1p}\boldsymbol{I}_{-1} + \boldsymbol{Z}_{-1n}\boldsymbol{I}_{1}^{*} + \boldsymbol{Z}_{-1s}\boldsymbol{I}_{3}^{*} \\ \boldsymbol{U}_{3} &= \boldsymbol{Z}_{3p}\boldsymbol{I}_{3} + \boldsymbol{Z}_{3n}\boldsymbol{I}_{-3}^{*} + \boldsymbol{Z}_{3s}\boldsymbol{I}_{-1}^{*} \\ \boldsymbol{U}_{-3} &= \boldsymbol{Z}_{-3p}\boldsymbol{I}_{-3} + \boldsymbol{Z}_{-3n}\boldsymbol{I}_{3}^{*} + \boldsymbol{Z}_{-3s}\boldsymbol{I}_{5}^{*} \\ &\cdots \end{aligned} \tag{26}$$

The relationship between the negative-sequence fundamental current and the positive-sequence third harmonic current is

$$\begin{aligned} \boldsymbol{I}_{-1}^{*} &= \frac{1}{\boldsymbol{Z}_{3s}}\left(\boldsymbol{U}_{3} - \boldsymbol{Z}_{3p}\boldsymbol{I}_{3} - \boldsymbol{Z}_{3n}\boldsymbol{I}_{-3}^{*}\right) \\ &= \frac{\boldsymbol{U}_{3}}{\boldsymbol{Z}_{3s}} - \frac{\boldsymbol{Z}_{3p}}{\boldsymbol{Z}_{3s}}\boldsymbol{I}_{3} - \frac{\boldsymbol{Z}_{3n}}{\boldsymbol{Z}_{3s}}\boldsymbol{I}_{-3}^{*} \end{aligned} \tag{27}$$

Since harmonics decrease rapidly with increasing order after modulations, the negative-sequence third harmonic current and the positive-sequence third harmonic voltage are usually ignored. These neglected parameters are regarded as the parameter errors of the harmonic current control. The robustness of the controller reduces their influence. Thus, the simplified relationship can be obtained as

$$\begin{aligned} \boldsymbol{I}_{-1} &\approx \left(\frac{\boldsymbol{r}_{p}}{-s\boldsymbol{L}_{s} + j3\omega_{e}\boldsymbol{L}_{s}} - \frac{\boldsymbol{l}_{p}}{\boldsymbol{L}_{s}}\right)\boldsymbol{I}_{3}^{*} \\ &\approx -\frac{\boldsymbol{L}_{p}}{\boldsymbol{L}_{s}}\boldsymbol{I}_{3}^{*} \end{aligned} \tag{28}$$

The effect of the impedance asymmetry is reduced by controlling the actual negative-sequence fundamental current reconstructed by the positive-sequence third harmonic current. Meanwhile, the measured negative-sequence fundamental current is employed to compensate for the measurement scaling error. Finally, the related harmonics caused by the impedance asymmetry and the current measurement error are suppressed in the motor.

C. HARMONIC CURRENT CONTROL

The complex vector design is a classical method of the fundamental current control [27]. The complex vector harmonic model established in this paper benefits the design of complex vector controllers, and the complex vector design can be extended to the harmonic current control. The PI regulators in MSF and PR regulators are similar and can be converted to each other. However, the complex vector model's design methods based on the PI regulators in MSF are clear. Therefore, the complex vector design of the PI regulators in MSF is adopted in the paper.

Firstly, the harmonic current controller is designed for the $(1-6N)^{\text{th}}$ and $(6N+1)^{\text{th}}$ order harmonic currents caused by spatial harmonics and the inverter nonlinearity. According to the harmonic impedances, the positive sequence impedance is the main component, and other impedances are ignored. Thus, the transfer function of the harmonic current controller is designed as

$$\boldsymbol{U}_{hc} = \omega_{hc}\frac{\boldsymbol{r}_{p} + s\boldsymbol{l}_{p} + jh\omega_{e}\boldsymbol{l}_{p}}{s}\boldsymbol{e}_{hc} \tag{29}$$

where $\boldsymbol{e}_{hc}$ and $\boldsymbol{U}_{hc}$ are the harmonic current error and harmonic voltage of the h^{th}-order harmonic controller, respectively; s is the Laplace operator; $||$ means absolute value; α_{hc} is the bandwidth factor of the h^{th}-order harmonic controller, and the bandwidth can be obtained as (it should be careful about bandwidth limits)

$$\omega_{hc} = \alpha_{hc}\left|\omega_{e}\right| \tag{30}$$

Considering the multiple PR regulators, the harmonic current is extracted from the error of the fundamental controller, which reduces the influence of the fundamental current. Moreover, the harmonic extraction can be removed. In order to conform to a conventional situation, a low-pass filter is adopted to extract the harmonic current in the paper. When the cut-off frequency is high, the filter can be ignored for the DC signal. The harmonic extraction is

$$\boldsymbol{I}_{hc} = -\frac{\beta_{hc}\left|\omega_{e}\right|}{s + \beta_{hc}\left|\omega_{e}\right|}\left(e^{-j(h-1)\theta_{e}}\boldsymbol{e}_{dq}\right) \tag{31}$$

where $\boldsymbol{e}_{dq}$ is the fundamental current error; $\boldsymbol{I}_{hc}$ and β_{hc} are the harmonic current and the filter coefficient of the h^{th}-order harmonic extraction, respectively.

Due to the increase in the harmonic order, the delay has a greater impact on the harmonic controller. Then the delay compensation is as follows

$$\boldsymbol{U}_{hdq} = e^{j(h-1)(\theta_{e}+\phi_{h})}\boldsymbol{U}_{hc} \tag{32}$$

where $\boldsymbol{U}_{hdq}$ is the h^{th}-order harmonic voltage injected into the fundamental controller; T_c is the control period of the controller, and the compensation angle of the h^{th}-order harmonic is

$$\phi_h = 1.5T_c(h-1)\omega_e \tag{33}$$

Thus, the harmonic current controller based on the complex vector design is shown in Fig. 3, which is a model-based parametric controller.

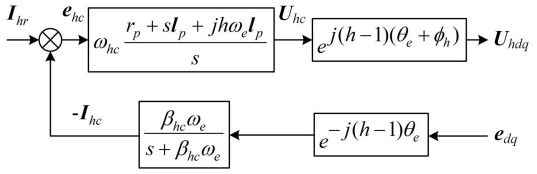

FIGURE 3. The diagram of the harmonic current controller.

Then, the harmonic current controller is designed for the actual negative-sequence fundamental current caused by the impedance asymmetry. Similarly, this harmonic current controller of the impedance asymmetry is designed as

$$\begin{aligned}
\boldsymbol{U}_{-1c} &= \omega_{-1c}\frac{\boldsymbol{r}_p + s\boldsymbol{l}_p - j\omega_e\boldsymbol{l}_p}{s}\boldsymbol{e}_{-1c} \\
\boldsymbol{I}_{3c} &= -\frac{\beta_{3c}\,|\omega_e|}{s+\beta_{3c}\,|\omega_e|}\left(e^{-j2\theta_e}\boldsymbol{e}_{dq}\right) \\
\boldsymbol{U}_{-1dq} &= e^{-j2(\theta_e+\phi_{-1})}\boldsymbol{U}_{-1c} \\
\boldsymbol{e}_{-1c} &= 0 - \boldsymbol{I}_{-1} = 0 + \frac{L_p}{L_s}\boldsymbol{I}^*_{3c}
\end{aligned} \tag{34}$$

where $\boldsymbol{e}_{-1c}$ and $\boldsymbol{I}_{-1}$ are the -1^{st}-order harmonic current error and the reconstructed -1^{st}-order harmonic current, respectively; $\boldsymbol{I}_{3c}$ and $\boldsymbol{U}_{-1c}$ are the 3^{rd}-order harmonic current and harmonic voltage of the -1^{st}-order harmonic controller, respectively; β_{3c} is the filter coefficient of the 3^{rd}-order harmonic extraction; $\boldsymbol{U}_{-1dq}$ is the -1^{st}-order harmonic voltage injected into the fundamental controller; α_{-1c} is a bandwidth factor of the -1^{st}-order harmonic controller and the bandwidth is $\omega_{-1c} = \alpha_{-1c}|\omega_e|$. The compensation angle of this harmonic is $\phi_{-1} = -1.5T_c2\omega_e$.

Therefore, the harmonic current controller of the impedance asymmetry is shown in Fig. 3.

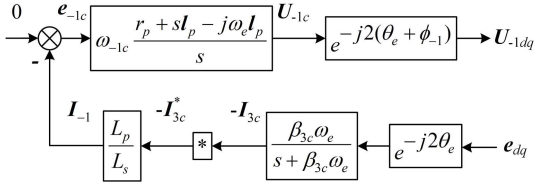

FIGURE 4. The diagram of the harmonic current controller considering the impedance asymmetry.

The harmonic current controller can effectively control the $(1-6N)^{\text{th}}$ and $(6N+1)^{\text{th}}$ order harmonic currents and the -1^{st}-order harmonic current. When the steady state is achieved, many harmonics generated by the saliency and impedance asymmetry converge to zero, which can be expressed as

$$\boldsymbol{I}_{1-} = 0, \quad \boldsymbol{I}_3 = 0, \ \boldsymbol{I}_{3-} = 0, \cdots \tag{35}$$

When the $(1-6N)^{\text{th}}$ and $(6N+1)^{\text{th}}$ order harmonic currents are injected, the related modulated harmonic currents are compensated by similar harmonic current controllers of the impedance asymmetry. However, the main purpose of this paper is to suppress current harmonics. Therefore, the controller only needs to compensate for the -1^{st}-order harmonic voltage caused by the impedance asymmetry.

D. MEASUREMENT ERROR COMPENSATION

Related current harmonics of current measurement errors are generated by the controller, which leads to many current harmonics by modulation effects in the motor. In analogy to the design of the harmonic current controller, the complex vector method is adopted to design current measurement error compensators in the paper. For current offset errors, the integral compensator and the direct current extraction in the measurement are designed as

$$\begin{aligned}
\boldsymbol{I}_{0mc} &= \frac{\omega_{0m}}{s}\boldsymbol{e}_{0m} \\
\boldsymbol{I}_{0c} &= -\frac{\beta_{0c}\,|\omega_e|}{s+\beta_{0c}\,|\omega_e|}\left(e^{j\theta_e}\boldsymbol{e}_{dq}\right)
\end{aligned} \tag{36}$$

where $\boldsymbol{e}_{0m}$ and $\boldsymbol{I}_{0mc}$ are the direct current error and the compensated direct current, respectively; $\boldsymbol{I}_{0c}$ and β_{0c} are the direct current and the filter coefficient of the direct current extraction, respectively; α_{0m} is the bandwidth factor of the current offset compensator, and the bandwidth is $\omega_{0m} = \alpha_{0m}|\omega_e|$.

The direct current is compensated in three-phase currents.

$$\begin{aligned}
I_{Amc} &= \frac{1}{2}\left(\boldsymbol{I}_{0mc} + \boldsymbol{I}^*_{0mc}\right) \\
I_{Bmc} &= \frac{1}{2}\left(e^{j\left(\theta-\frac{2}{3}\pi\right)}\boldsymbol{I}_{0mc} + e^{-j\left(\theta-\frac{2}{3}\pi\right)}\boldsymbol{I}^*_{0mc}\right)
\end{aligned} \tag{37}$$

Therefore, the offset compensator is shown in Fig. 5. The direct current in the measurement is extracted by the error of the fundamental current controller, and then offset errors of phase A and B are compensated.

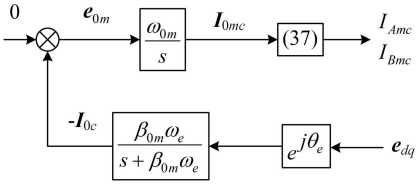

FIGURE 5. The diagram of the current offset compensator.

The current measurement scaling error is handled similarly, and the scaling error compensator is designed as

$$\begin{aligned}
k_c &= \frac{\omega_{-1m}}{2s}e_{-1m} \\
\boldsymbol{I}_{-1c} &= -\frac{\beta_{-1c}\,|\omega_e|}{s+\beta_{-1c}\,|\omega_e|}\left(e^{j2\theta_e}\boldsymbol{e}_{dq}\right)
\end{aligned} \tag{38}$$

where $\boldsymbol{e}_{-1m}$ and k_c are the error of the scaling error compensator and the compensated scaling gain, respectively; $\boldsymbol{I}_{-1c}$ and β_{-1c} are the -1^{st} order harmonic current and the filter coefficient of the harmonic extraction, respectively; α_{-1m} is the bandwidth factor of the scaling gain compensator and the bandwidth is $\omega_{-1m} = \alpha_{-1m}|\omega_e|$.

The relationship between the error of the compensator and the difference of scaling errors can be calculated as

$$\boldsymbol{e}_{-1m} = \frac{1}{I_{rs}^2 + \varepsilon}\left(1 - e^{j\frac{2}{3}\pi}\right)\boldsymbol{I}_{rdq}^{*}\boldsymbol{I}_{-1c} \approx k_{A\Delta} - k_{B\Delta} \tag{39}$$

where $\boldsymbol{I}_{rdq}$ and I_{rs} are the reference and the amplitude of the fundamental current control, respectively; ε is a small constant to avoid dividing by zero.

The scaling gain is compensated in three phases as

$$\begin{aligned} k_{Am} &= 1 - k_c \\ k_{Bm} &= 1 + k_c \end{aligned} \tag{40}$$

Therefore, the scaling error compensator is shown in Fig. 6. The negative-sequence 1^{st} harmonic current is extracted by the error of the fundamental current controller. Then the negative-sequence scaling error of phase A and B is compensated.

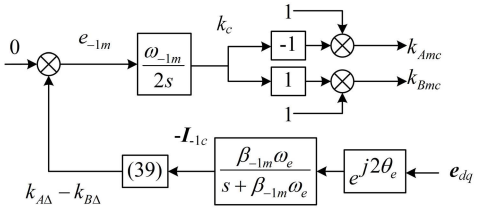

FIGURE 6. The diagram of the scaling error compensator.

E. OVERALL CONTROL STRATEGY

In order to reduce the influence of the fundamental control on the harmonic current extraction, a two-degree-of-freedom (2DOF) fundamental current controller is designed based on the complex vector model. Firstly, the fundamental current error is

$$\boldsymbol{e}_{dq} = \boldsymbol{I}_{rdq} - \boldsymbol{I}_{dq} \tag{41}$$

where $\boldsymbol{I}_{dq}$ is the current in the synchronous frame.

Secondly, the reference transfer function is defined as

$$G_r = \frac{\boldsymbol{I}_{rdq}}{\boldsymbol{I}_{r1}} = \frac{\omega_{cr}}{s + \omega_{cr}} \tag{42}$$

where $\boldsymbol{I}_{r1}$ is the actual reference in the synchronous frame; ω_{cr} is the bandwidth of the reference response.

Then, the input-output relationship of disturbance is defined as

$$\begin{aligned} \boldsymbol{U}_{1dq} &= G_{c1}\boldsymbol{e}_{dq} + G_{c2}\boldsymbol{e}_{dq}^{*} \\ &= \omega_c \frac{\boldsymbol{r}_p + s\boldsymbol{l}_p + j\omega_e\boldsymbol{l}_p}{s}\boldsymbol{e}_{dq} \\ &\quad + \omega_c \frac{sL_s + j\omega_e L_s}{s}\boldsymbol{e}_{dq}^{*} \end{aligned} \tag{43}$$

where $\boldsymbol{G}_{c1}$ and $\boldsymbol{G}_{c2}$ are the positives sequence controller and the saliency controller, respectively; ω_c is the bandwidth of the disturbance response.

This fundamental current controller is a multiple input and multiple output (MIMO) controller considering motor saliency, and it is equivalent to converting the complex vector form into the vector form. Finally, the reference feedforward is defined as

$$\begin{aligned} \boldsymbol{U}_{rdq} &= (\boldsymbol{r}_p + s\boldsymbol{l}_p + j\omega_e\boldsymbol{l}_p)\boldsymbol{I}_{rdq} \\ &\quad + (sL_s + j\omega_e L_s)\boldsymbol{I}_{rdq}^{*} \end{aligned} \tag{44}$$

The closed-loop response of the reference is different from that of the disturbance, and this fundamental current controller is a 2DOF controller [15]. When the reference bandwidth is consistent with the disturbance bandwidth, the fundamental current controller can be simplified to the classical complex vector controller.

Therefore, the overall scheme of the modulation-based current harmonic controller is shown in Fig. 7, which consists of the current measurement error compensator, the harmonic current controller, and the fundamental current controller. In order to verify the effect of current measurement errors, the measurement errors are also included in the controller.

These controllers and compensators are parametric in design, where the selection of parameters is relatively simple. Higher bandwidth means faster response, but the system robustness is reduced. In the fundamental controller, the reference bandwidth needs to be smaller than the disturbance bandwidth. The bandwidth of the harmonic current controller needs to be within the bandwidth of the fundamental controller, and the filter bandwidth of the harmonic extraction is larger than the bandwidth of the harmonic current control to avoid the oscillation caused by the filter delay. When the harmonic frequency is close to the fundamental frequency, the controllers or compensators can be affected by the fundamental controller, and the bandwidth needs to be reduced. The measurement error usually varies slowly, hence the bandwidth and the filter coefficient in the measurement error compensator are smaller than the bandwidth of the harmonic current controller. Generally, model inaccuracy and time delays may cause instability and oscillation in the control system. Better robustness can be achieved with a small bandwidth when performance requirements are satisfied.

IV. EXPERIMENTAL VALIDATION

The control strategy has been experimentally verified on a laboratory platform which includes dSPACE (DS1103), a three-phase inverter, a DC power supply, and a PMSM in Fig. 8. Parameters of an interior permanent-magnet synchronous machine (IPMSM) and the drive are shown in Table 1. Since the phase resistance is small, an asymmetric impedance is generated by the additional copper wire connection on phase C (the resistance of phase C is approximately 90 mΩ). In practice, the resistance of the connection may not be equal. Thus this asymmetry can represent the effectiveness of the control strategy proposed in the paper.

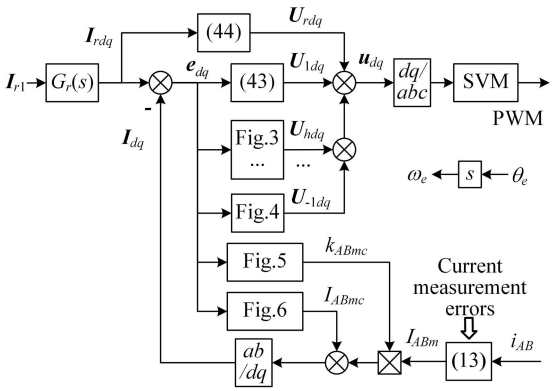

FIGURE 7. The overall scheme of the modulation-based current harmonic controller.

TABLE 1. Parameters of machine and drive.

Parameters	Values
Number of pole pairs	3
Stator resistance R_s	57 mΩ
D-axis inductance L_d	0.63 mH
Q-axis inductance L_q	1.39 mH
Rated speed	1000 rpm
Rated torque	55 Nm
DC linkage voltage	100 V
Sampling& switching frequency	4 kHz

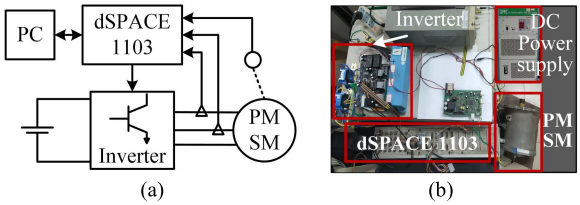

FIGURE 8. Laboratory test platform. (a) Diagram of the platform. (b) Pictures of the platform.

TABLE 2. Parameters of controller.

Parameters	Values	Parameters	Values
ω_{cr}	2π·20 Hz	ω_c	2π·20 Hz
α_{hc}	0.25	β_{hc}	0.5
α_{-1c}	0.05	β_{-1c}	0.1
α_{-1m}	0.05	β_{-1m}	0.1
α_{0m}	0.05	β_{0m}	0.1
$k_{A\Delta}$	-0.05	$k_{B\Delta}$	0.05
i_{Adc}	1 A	i_{Bdc}	-1 A

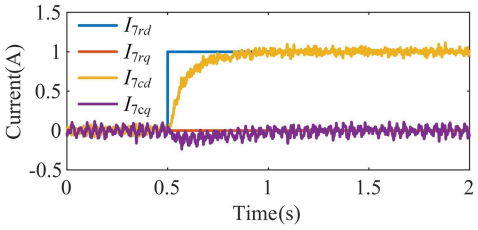

FIGURE 9. The current response of the 7th order harmonic current.

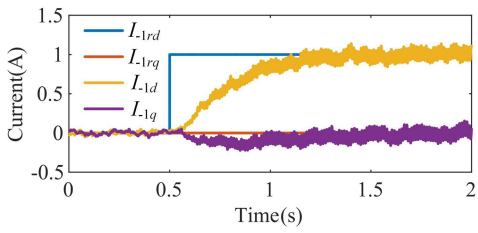

FIGURE 10. The current response of the −1st-order harmonic current controller considering the impedance asymmetry.

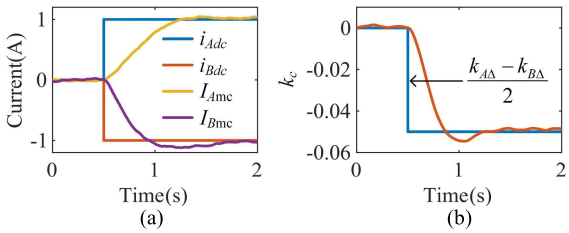

FIGURE 11. The current measurement error compensation. (a) The current offset compensation. (b) The scaling error compensation.

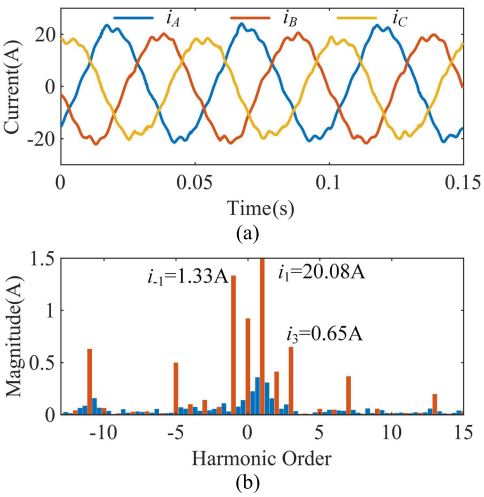

FIGURE 12. Waveforms and spectra of measured current without the harmonic current control. (a) Phase current. (b) Spectrum.

According to the design principle and experimental tests, some parameters of the controller are shown in Table 2. Based on the switching frequency and time delays, the fundamental bandwidth is determined, and other bandwidths are reduced. When motor parameters are known, we determine the parameters of the entire controller.

To verify the harmonic current controller, the speed is controlled to 400 rpm, and the reference of the d-axis is −20 A. The harmonic current controller need to suppress the main $(1-6N)^{\text{th}}$ and $(6N+1)^{\text{th}}$ order harmonic currents, and thus these harmonic orders are −11, −5, 7, and 13. Parameters of the controller are shown in Table 2. We take the 7^{th}-order harmonic current as an example, and other current harmonics and errors are compensated. The harmonic current references are I_{7rd} and I_{7rq}, and the harmonic current feedbacks are I_{7cd}

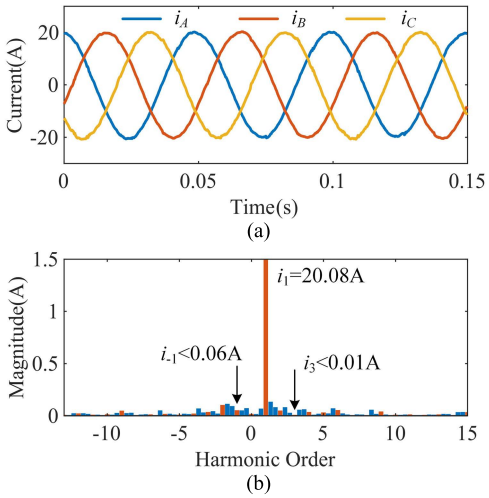

FIGURE 13. Waveforms and spectra of measured current with the harmonic current control. (a) Phase current. (b) Spectrum.

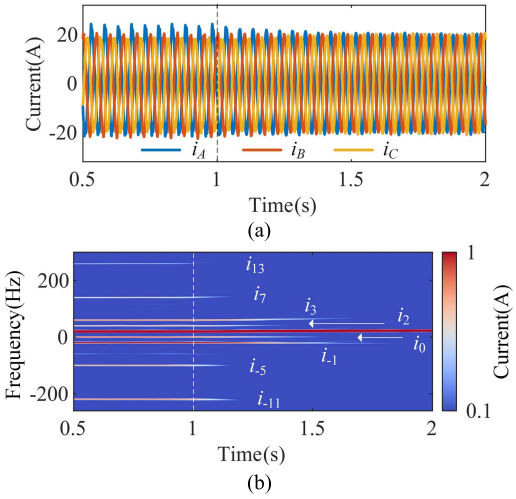

FIGURE 14. Waveforms and time-frequency spectrum of measured current when the harmonic current controller is enabled at 1s. (a) Phase current. (b) Time-frequency spectrum.

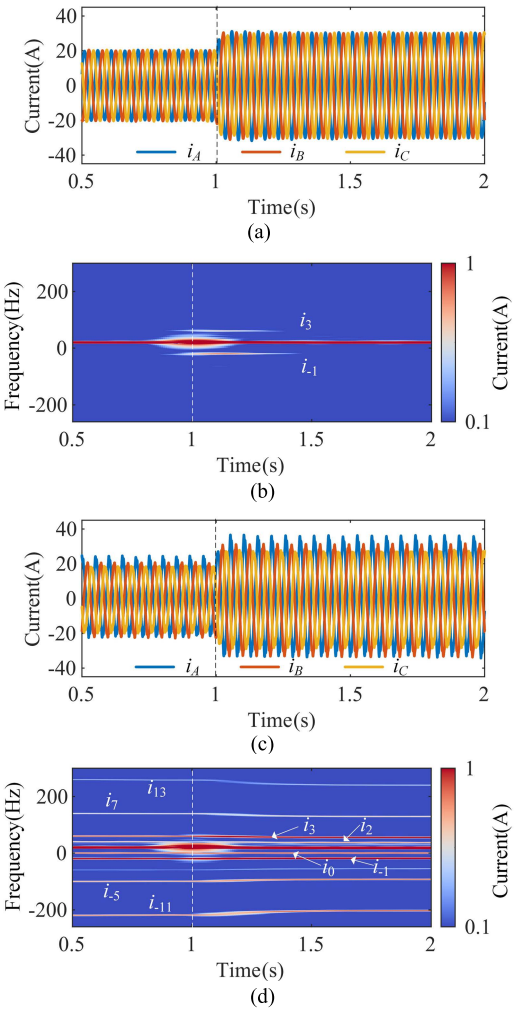

FIGURE 15. Waveforms and time-frequency spectrum of measured current when the reference of the d-axis steps at 1s. (a) Phase current with the proposed strategy. (b) Time-frequency spectrum with the proposed strategy. (c) Phase current without the proposed strategy. (d) Time-frequency spectrum without the proposed strategy.

and I_{7cq}. Then I_{7rd} steps to 1 A when the time is 0.5 s, and the harmonic current response is shown in Fig. 9. The result illustrates that currents take about 0.2 s to reach a steady state, and the bandwidth is about 5 Hz. The design is basically consistent with the test result, which shows the correctness of the design method.

In the same case, the harmonic current controller of the asymmetry is verified. The harmonic frequency of the impedance asymmetry is close to the fundamental frequency. Thus parameters of this controller are smaller, as shown in Table 2. The harmonic current references are I_{-1rd} and I_{-1rq}, and the harmonic current feedbacks are I_{-1d} and I_{-1q}. Then I_{-1rd} steps to 1 A when the time is 0.5 s, and the harmonic current response is shown in Fig. 10. As a result, the currents take about 1 s to reach a steady state, and the bandwidth is about 1 Hz. The harmonic current controller can control the negative-sequence fundamental current by the reconstruction of the 3rd-order harmonic current.

In the same case, we verify the current measurement error compensation. The current measurement errors usually vary slowly, and thus the parameters are smaller, as shown in Table 2. The measurement errors in the controller step when time is 0.5 s, and the responses are shown in Fig. 11. As a result, the error compensation takes about 1s to reach a steady state, and the bandwidth is about 1 Hz.

To verify the steady performance, the speed and the current reference are the same as the previous case, and the parameters are shown in Table 2. Then the actual three-phase current and its spectrum before and after the harmonic current control are compared, as shown in Fig. 12 and Fig. 13. As illustrated in Fig. 12, when the system includes current measurement errors and asymmetry, there are the $(1-6N)^{\text{th}}$ and $(6N+1)^{\text{th}}$ order harmonic component, the DC component, the -1^{st}-order harmonic component, and modulated

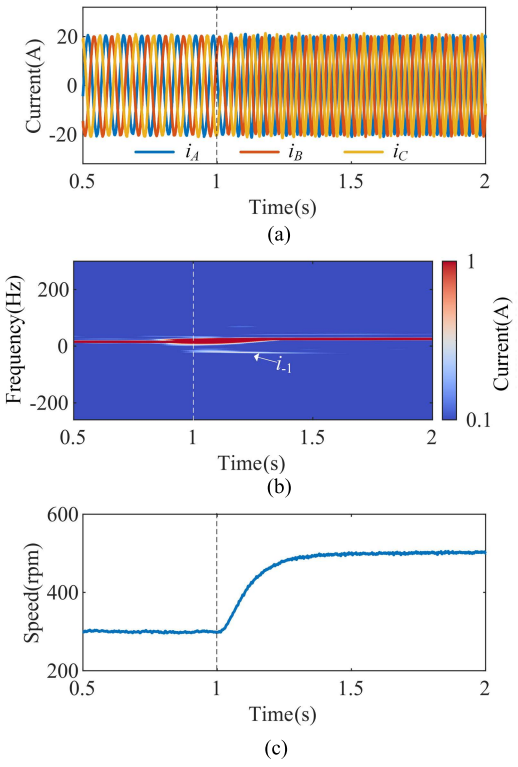

FIGURE 16. Waveforms, time-frequency spectrum of measured current, and speed response when the speed steps at 1s. (a) Phase current. (b) Time-frequency spectrum. (c) Speed response.

harmonic components. The -1^{st}-order harmonic component is 1.33 A, and the 3^{rd}-order harmonic component modulated by the saliency is 0.65 A. The DC component is 0.92 A and the 2^{nd}-order harmonic component modulated by the saliency is 0.41 A. The maximum component among the $(6N+1)^{th}$-order harmonics is the -11^{th}-order component, which is 0.63 A. When the control strategy is applied, Fig. 13 shows that the $(1-6N)^{th}$ and $(6N+1)^{th}$ order harmonic component, the DC component, and the -1^{st}-order harmonic component in the motor are controlled to below 0.1 A. Then related harmonics generated by the modulation also tend to zero. Thus, the results show that the control strategy is effective in suppressing harmonic currents.

To verify the dynamic performance, the conditions are the same as the previous case. The harmonic current controller is enabled at 1s. Then the time-frequency spectrum of the actual current is analyzed by a short-time Fourier transform. The actual current and its time-frequency spectrum are shown in Fig. 14. As a result, the $(1-6N)^{th}$ and $(6N+1)^{th}$ order harmonic components can be suppressed to below 0.1 A within 0.5 s. Meanwhile, harmonic components of the impedance asymmetry and current measurement errors can be suppressed to below 0.1 A within 1 s. The result indicates the effectiveness of the proposed control strategy.

In order to verify the effect of the fundamental current, the speed is controlled to 400 rpm. The reference of the d-axis steps from -20 A to -30 A at 1 s. The actual three-phase current and its time-frequency spectrum are compared with and without the proposed strategy, as shown in Fig. 15. As a result, with the proposed strategy, the -1^{st}-order harmonic component and the 3^{rd}-order harmonic component generated by the asymmetric resistance can increase with the reference step. Then these current harmonics can be suppressed after 1.5 s. Without the proposed strategy, these current harmonics are always present at all times. The result indicates the effectiveness of the control strategy when the fundamental current steps.

To verify the effect of the speed, the reference of the d-axis is -20 A, and the bandwidth of the speed controller is 2 Hz. Then the speed reference steps from 300 rpm to 500 rpm at 1s. The actual three-phase current, its time-frequency spectrum, and the speed response are shown in Fig. 16. As a result, the harmonic components can be suppressed when the speed steps. The result indicates the effectiveness of the control strategy when the speed steps.

V. CONCLUSION

In this paper, a novel modulation-based current harmonic control strategy is proposed. The impedance asymmetry control employs the negative-sequence fundamental current reconstructed by the saliency modulation. Meanwhile, current measurement errors are compensated, and harmonic currents generated by spatial harmonics and the inverter nonlinearity are suppressed. The experiment shows that the control strategy is effective in steady states and dynamics, and various harmonics, as well as other modulated harmonics, are suppressed.

REFERENCES

[1] M. L. De Klerk and A. K. Saha, "A comprehensive review of advanced traction motor control techniques suitable for electric vehicle applications," *IEEE Access*, vol. 9, pp. 125080–125108, 2021, doi: 10.1109/ACCESS.2021.3110736.
[2] W. Cao, B. C. Mecrow, G. J. Atkinson, J. W. Bennett, and D. J. Atkinson, "Overview of electric motor technologies used for more electric aircraft (MEA)," *IEEE Trans. Ind. Electron.*, vol. 59, no. 9, pp. 3523–3531, Sep. 2012, doi: 10.1109/TIE.2011.2165453.
[3] J. H. Lee and S. K. Sul, "Inverter nonlinearity compensation through deadtime effect estimation," *IEEE Trans. Power Electron.*, vol. 36, no. 9, pp. 10684–10694, Sep. 2021, doi: 10.1109/TPEL.2021.3061285.
[4] H. Kim, Y. Han, K. Lee, and S. Bhattacharya, "A sinusoidal current control strategy based on harmonic voltage injection for harmonic loss reduction of PMSMs with non-sinusoidal back-EMF," *IEEE Trans. Ind. Appl.*, vol. 56, no. 6, pp. 7032–7043, Nov. 2020, doi: 10.1109/TIA.2020.3016210.
[5] Y. Xu, N. Parspour, and U. Vollmer, "Torque ripple minimization using online estimation of the stator resistances with consideration of magnetic saturation," *IEEE Trans. Ind. Electron.*, vol. 61, no. 9, pp. 5105–5114, Sep. 2014, doi: 10.1109/TIE.2013.2279378.
[6] H. S. Jung, S. H. Hwang, J. M. Kim, C. U. Kim, and C. Choi, "Diminution of current-measurement error for vector-controlled AC motor drives," *IEEE Trans. Ind. Appl.*, vol. 42, no. 5, pp. 1249–1256, Sep. 2006, doi: 10.1109/TIA.2006.880904.
[7] G. Feng, C. Lai, and N. C. Kar, "Practical testing solutions to optimal stator harmonic current design for PMSM torque ripple minimization using speed harmonics," *IEEE Trans. Power Electron.*, vol. 33, no. 6, pp. 5181–5191, Jun. 2018, doi: 10.1109/TPEL.2017.2738613.
[8] P. L. Chapman and S. D. Sudhoff, "A multiple reference frame synchronous estimator/regulator," *IEEE Trans. Energy Convers.*, vol. 15, no. 2, pp. 197–202, Jun. 2000, doi: 10.1109/60.867000.
[9] G. Liu, B. Chen, K. Wang, and X. Song, "Selective current harmonic suppression for high-speed PMSM based on high-precision harmonic detection method," *IEEE Trans. Ind. Informat.*, vol. 15, no. 6, pp. 3457–3468, Jun. 2019, doi: 10.1109/TII.2018.2873652.

[10] J. Qu, J. Jatskevich, C. Zhang, and S. Zhang, "Torque ripple reduction method for permanent magnet synchronous machine drives with novel harmonic current control," *IEEE Trans. Energy Convers.*, vol. 36, no. 3, pp. 2502–2513, Sep. 2021, doi: 10.1109/TEC.2021.3056557.
[11] L. Yan, Z.-Q. Zhu, J. Qi, Y. Ren, C. Gan, S. Brockway, and C. Hilton, "Suppression of major current harmonics for dual three-phase PMSMs by virtual multi three-phase systems," *IEEE Trans. Ind. Electron.*, vol. 69, no. 6, pp. 5478–5490, Jun. 2022, doi: 10.1109/TIE.2021.3091922.
[12] D. N. Zmood, D. G. Holmes, and G. H. Bode, "Frequency-domain analysis of three-phase linear current regulators," *IEEE Trans. Ind. Appl.*, vol. 37, no. 2, pp. 601–610, Mar. 2001, doi: 10.1109/28.913727.
[13] A. G. Yepes, F. D. Freijedo, O. Lopez, and J. Doval-Gandoy, "High-performance digital resonant controllers implemented with two integrators," *IEEE Trans. Power Electron.*, vol. 26, no. 2, pp. 563–576, Feb. 2011, doi: 10.1109/TPEL.2010.2066290.
[14] A. G. Yepes, J. Malvar, A. Vidal, O. López, and J. Doval-Gandoy, "Current harmonics compensation based on multiresonant control in synchronous frames for symmetrical n-phase machines," *IEEE Trans. Ind. Electron.*, vol. 62, no. 5, pp. 2708–2720, May 2015, doi: 10.1109/TIE.2014.2365155.
[15] Z. Pan, F. Dong, J. Zhao, L. Wang, H. Wang, and Y. Feng, "Combined resonant controller and two-degree-of-freedom PID controller for PMSLM current harmonics suppression," *IEEE Trans. Ind. Electron.*, vol. 65, no. 9, pp. 7558–7568, Sep. 2018, doi: 10.1109/TIE.2018.2793232.
[16] P. Mattavelli, L. Tubiana, and M. Zigliotto, "Torque-ripple reduction in PM synchronous motor drives using repetitive current control," *IEEE Trans. Power Electron.*, vol. 20, no. 6, pp. 1423–1431, Nov. 2005, doi: 10.1109/TPEL.2005.857559.
[17] Z. Tang and B. Akin, "A new LMS algorithm based deadtime compensation method for PMSM FOC drives," *IEEE Trans. Ind. Appl.*, vol. 54, no. 6, pp. 6472–6484, Nov. 2018, doi: 10.1109/TIA.2018.2853045.
[18] L. Wang, Z. Q. Zhu, H. Bin, and L. M. Gong, "Current harmonics suppression strategy for PMSM with nonsinusoidal back-EMF based on adaptive linear neuron method," *IEEE Trans. Ind. Electron.*, vol. 67, no. 11, pp. 9164–9173, Nov. 2020, doi: 10.1109/TIE.2019.2955414.
[19] J. Lu, Y. Hu, J. Liu, J. Wang, and P. Li, "Fixed-point sampling strategy for estimation on current measurement errors in IPMSM drives," *IEEE Trans. Power Electron.*, vol. 36, no. 5, pp. 5748–5759, May 2021, doi: 10.1109/TPEL.2020.3031352.
[20] Q. N. Trinh, P. Wang, Y. Tang, L. H. Koh, and F. H. Choo, "Compensation of DC offset and scaling errors in voltage and current measurements of three-phase AC/DC converters," *IEEE Trans. Power Electron.*, vol. 33, no. 6, pp. 5401–5414, Jun. 2018, doi: 10.1109/TPEL.2017.2734809.
[21] K.-W. Lee and S.-I. Kim, "Dynamic performance improvement of a current offset error compensator in current vector-controlled SPMSM drives," *IEEE Trans. Ind. Electron.*, vol. 66, no. 9, pp. 6727–6736, Sep. 2019, doi: 10.1109/TIE.2018.2877162.
[22] M. Kim, S.-K. Sul, and J. Lee, "Compensation of current measurement error for current-controlled PMSM drives," *IEEE Trans. Ind. Appl.*, vol. 50, no. 5, pp. 3365–3373, Sep. 2014, doi: 10.1109/TIA.2014.2301873.
[23] M. C. Harke, J. M. Guerrero, M. W. Degner, F. Briz, and R. D. Lorenz, "Current measurement gain tuning using high-frequency signal injection," *IEEE Trans. Ind. Appl.*, vol. 44, no. 5, pp. 1578–1586, Sep. 2008, doi: 10.1109/TIA.2008.2002170.
[24] P. Xiao, K. A. Corzine, and G. K. Venayagamoorthy, "Multiple reference frame-based control of three-phase pwm boost rectifiers under unbalanced and distorted input conditions," *IEEE Trans. Power Electron.*, vol. 23, no. 4, pp. 2006–2017, Jul. 2008, doi: 10.1109/TPEL.2008.925205.
[25] A. H. Abosh, Z. Zhu, and Y. Ren, "Reduction of torque and flux ripples in space vector modulation-based direct torque control of asymmetric permanent magnet synchronous machine," *IEEE Trans. Power Electron.*, vol. 32, no. 4, pp. 2976–2986, Apr. 2017, doi: 10.1109/TPEL.2016.2581026.
[26] L. Harnefors, "Modeling of three-phase dynamic systems using complex transfer functions and transfer matrices," *IEEE Trans. Ind. Electron.*, vol. 54, no. 4, pp. 2239–2248, Aug. 2007, doi: 10.1109/TIE.2007.894769.
[27] F. Briz, M. W. Degner, and R. D. Lorenz, "Analysis and design of current regulators using complex vectors," *IEEE Trans. Ind. Appl.*, vol. 36, no. 3, pp. 817–825, May 2000, doi: 10.1109/28.845057.

HAO LIN was born in Fujian, China, in 1991. He received the B.Sc. degree in electrical engineering from Chongqing University, Chongqing, China, in 2014, where he is currently pursuing the Ph.D. degree. His current research interests include nonlinear current control and harmonic control of PMSMs.

YONG LIAO received the M.Eng. degree in electrical machinery and the Ph.D. degree in power system control from Chongqing University, Chongqing, China, in 1988 and 1997, respectively. In 1998, he participated with the Global Development Program of Rockwell Automation, Milwaukee, WI, USA. From 2001 to 2002, he was a Visiting Professor at Northumbria University, Newcastle, U.K. He is currently a Professor of electrical machinery and apparatus at Chongqing University. His research interest includes the control of doubly-fed electrical machines as used in renewable energy systems, including wind and micro-hydro generators.

LUOCHENG YAN received the B.Sc. and M.Sc. degrees in electrical engineering from the School of Electrical Engineering, Chongqing University, Chongqing, China, in 2016 and 2019, respectively. He is currently pursuing the Ph.D. degree in electrical engineering with The University of Sheffield, Sheffield, U.K. His research interest includes high performance drive and control of three-phase and multi three-phase permanent magnet synchronous machines.

FU LI was born in Henan, China, in 1991. He received the B.Sc. and Ph.D. degrees in electrical engineering from Chongqing University, Chongqing, China, in 2013 and 2018, respectively. From 2018 to 2022, he was a Motor Control Engineer at SZ DJI Technology Company Ltd. He is currently a Lecturer at Xiangtan University. His research interests include high-speed PMSM drives, and sensorless and fault-tolerant control of PM motors.

YIXIAO FENG was born in Henan, China, in 1992. He received the B.Sc. degree in electrical engineering from Chongqing University, Chongqing, China, in 2014, where he is currently pursuing the Ph.D. degree. His current research interests include fault-tolerant control and harmonic elimination of multiphase PM motors.